Journal of Arid Environments 220 (2024) 105096

Contents lists available at ScienceDirect

Journal of Arid Environments

journal homepage: www.elsevier.com/locate/jaridenv

First measurements of electric field variability during fog events in the United Arab Emirates

Narendra Nelli [a], Diana Francis [a,*], Ricardo Fonseca [a], Olivier Masson [b], Mamadou Sow [c], Emmanuel Bosc [d]

[a] Environmental and Geophysical Sciences (ENGEOS) Lab, Earth Science Department, Khalifa University, P.O. Box 127788, Abu Dhabi, United Arab Emirates
[b] Institut de Radioprotection et de Sûreté Nucléaire (IRSN), PSE-ENV, SERPEN, LEREN, Cadarache, 13115, Saint Paul-Lez-Durance, France
[c] Institut de Radioprotection et de Sûreté Nucléaire (IRSN), PSN-RES, SCA, LPMA, F-91400, Saclay, France
[d] Federal Authority for Nuclear Regulation (FANR), P.O. Box: 112021, Abu Dhabi, United Arab Emirates

ARTICLE INFO

Keywords:
Atmospheric electric field
Fog
Visibility
Aerosols
Hyper-arid region
United Arab Emirates

ABSTRACT

For the first time, the changes in the atmospheric electric field (E_z) during foggy conditions is studied in a hyper-arid region; the United Arab Emirates (UAE), using comprehensive measurements during the *Wind-blown Sand Experiment (WISE)-UAE*. The longer the fog persists, the more variable E_z becomes, primarily due to the fog's ability to absorb and redistribute the charges of the atmospheric small ions. This absorption alters the ion balance, affecting electrical conductivity within the atmosphere, which in turn leads to sustained alterations in E_z. A record high E_z value of 2571 V m^{-1} was measured during a long-lasting fog event. E_z values returned to normal during the fog dissipation phase. The results of this work can be applied to develop techniques for fog harvesting and to improve fog forecasting by accounting for the effect of the electric field on fog lifetime and characteristics.

1. Introduction

Fog is a prevalent weather phenomenon several arid regions such as the Empty Quarter desert in the United Arab Emirates (UAE), positioned on the northeastern side of the Arabian Peninsula. Even though it is primarily an arid country with desert landscapes dominating its terrain, most events causing visibility to drop below 1 km in the UAE are attributed to condensation processes rather than dust occurrence (Aldababseh and Temimi, 2017). Except along the east coast, fog incidences in the UAE typically increase during the cooler months of December to March (Mohan et al., 2020) and are predominantly due to radiative cooling processes, as outlined in Weston et al. (2021). During daytime, sea-breeze circulations transport moisture-laden marine air inland. As night falls, the rapid cooling of the surface engenders a shift from the sea-breeze to a gentler land-breeze, leading to the entrapment of the moist air inland. The potent radiative cooling instigates the creation of a stable boundary layer, bringing the entrapped air masses to saturation and culminating in the formation of fog (Temimi et al., 2020a). This formation process is further augmented by the presence of ambient aerosol particles, both natural and anthropogenic (Jia et al., 2019; Nelli et al., 2021a).

In-situ measurements of fog droplets carried out over western UAE, reveal a bimodal distribution in droplet number concentration, with modes at 4.5 μm and 22–25 μm (Abida et al., 2023; Nelli et al., 2022; Weston et al., 2022). The primary factors contributing to fog creation in the region encompass local-scale circulations (land-sea-breeze), calm conditions during the night, and a stable nocturnal boundary layer. Another substantial contributing factor is atmospheric rivers, which are elongated, narrow corridors of elevated water vapor content that can also act as moisture providers for fog events (Francis et al., 2022; Verma et al., 2022), and whose frequency is increasing in the Middle East (Massoud et al., 2020; Esfandiari and Rezaei, 2022). Fonseca et al. (2023) reported an increasing trend both in frequency and duration of consecutive foggy days in the UAE stressing out the need for a more accurate fog forecasting systems to alleviate the risks fog poses on the daily life of people in these regions.

Accurate fog forecasting is essential, serving critical roles in managing water resources and minimizing the hazardous impacts on transport networks (Gultepe and Milbrandt, 2007, 2009; Westcott and Kristovich, 2009; de Villiers and van Heerden, 2007; Stolaki et al., 2009). However, deciphering accurate fog data from numerical weather prediction models continues to be a significant challenge (Bergot et al.,

* Corresponding author.
E-mail address: diana.francis@ku.ac.ae (D. Francis).

https://doi.org/10.1016/j.jaridenv.2023.105096
Received 26 September 2023; Received in revised form 1 November 2023; Accepted 2 November 2023
Available online 26 November 2023

2007, 2015; Yang et al., 2010; Branch et al., 2021), prompting the development of a variety of methods to address this. The endeavor to forecast fog has witnessed several attempts in the United Arab Emirates, employing the Weather Research and Forecasting (WRF) model. For instance, Valappil et al. (2019) applied bias correction methods to the 2-m air temperature to rectify the cold bias prevalent during nighttime and early morning hours. Nelli et al. (2020) refined the aerodynamic roughness length to forecast wind speed and 2-m air temperature with enhanced accuracy. Temimi et al. (2020b) updated the soil texture and land use land cover in the WRF model, further reducing the nighttime cold temperature bias. Additionally, Weston et al. (2021) proposed a multi-rule-based method, utilizing threshold values of multiple variables for diagnosing fog in arid regions, achieving a probability of detection of 0.62.

The landscape of monitoring and predicting fog has evolved, moving beyond traditional in-situ observations thanks to technological advancements. A host of new tools and methodologies have been adopted for an in-depth study of fog and its associated factors. Fog forecasting follows two primary routes: statistical and dynamical forecasting. Traditional statistical methods were built on various analyses, including classification, correlation, and regression. The advancement of computational power has paved the way for emerging statistical methods, leveraging deep learning and machine learning neural network tools such as CNN (Convolution Neural Network), RNN (Recurrent Neural Network), and ANN (Artificial Neural Network), which are proving to be promising tools in fog research. For the construction of a robust fog forecast model, it is imperative to identify as many influential variables as possible relating to fog occurrence, duration, and intensity. The present study introduces electric field variability as one such parameter. We aim to bridge the existing gap by offering a thorough analysis of electric field behavior under foggy conditions. By deepening the understanding of how fog events affect electric field variability, we aspire to contribute valuable insights that can be incorporated into forecasting models, thus enhancing their accuracy and reliability. The progress in fog forecasting, facilitated by our research, is set to be instrumental in mitigating the adverse effects of unexpected fog events and in fostering improved preparedness and response strategies across various sectors.

Cosmic rays and terrestrial radioactivity generate ambient ions, making the atmosphere electrically conductive. The conductivity of the atmosphere (σ) is determined by the mobility (μ) and concentration of ambient ions (n). Larger and slower ions reduce the conductivity compared to faster and lighter ones. An increase in the number density of suspended water droplets decreases the electrical conductivity of the air by removing small ions through attachment (Bennett and Harrison, 2009; R G Harrison, 2003). The conductivity is therefore related to the mobility and the concentrations of ions. The total conductivity (σ_T) from the negative (−) and positive (+) ions in the atmosphere is defined by:

$$\sigma_T = \sigma_+ + \sigma_- = e\left(\sum \mu_+ n_+ + \sum \mu_- n_-\right)$$

where e represents the elementary charge.

According to Ohm's law, the current density J_z is a product of the electrical conductivity and the electric field strength E_z, where z denotes the vertical component. Mathematically, this is represented as $J_z = \sigma E_z$. When atmospheric factors lead to a decrease in σ, such as the increase in the number density of suspended water droplets, and if J is held constant, the electric field strength E_z compensates for the decreasing σ by increasing. Fog represents a unique natural environment for exploring the physics of water droplet charging, the aeroelectric state of the boundary layer, and their interplay with cloud formation (Anisimov et al., 2005). In fog or clouds, where the air is filled with droplets, these small ions attach to the droplets, decreasing the local air's conductivity. The extent of this conductivity reduction is influenced by the droplets' number, size, and separation distance (Bennett and Harrison, 2009; Ambaum et al., 2022). The longer the fog persists, the more time there is for fog droplets to interact with ambient ions, leading to more prolonged and extensive alterations in the atmospheric electric field, and consequently resulting in greater variability. This variability in the electric field can affect droplet collision-coalescence and the evolution of cloud droplet size distributions.

While the prolonged duration of fog leads to increased interactions between droplets and ambient ions, resulting in extended alterations in the atmospheric electric field, the specific magnitude and nature of this variability require further exploration. The atmospheric electric field, influenced by myriad factors, becomes increasingly complex in foggy conditions. Although our understanding of the variability of the atmospheric electric field in foggy conditions is advancing, the intricate dynamics of this relationship are still unfolding, necessitating continued research. Studies such as those by Guo and Xue (2021), Nicoll et al. (2022), and Yair and Yaniv (2023) have provided invaluable insights. For instance, Guo and Xue (2021) found that electric charges enhance the collision efficiency, especially between small water droplets, in line with the results of Ambaum et al. (2022). Fog, by reducing visibility and exhibiting spatial variability in its intensity, can also amplify the local electric field across different areas (Nicoll et al., 2022; Yair and Yaniv, 2023). Moreover, typical influencers of the electric field, such as ground structures, lose their efficacy due to the fog's attenuating effects. As a result, the fog's duration and intensity become critical determinants of the electric field's behavior. Nevertheless, achieving a comprehensive understanding, especially within unique environments like the UAE's Empty Quarter desert, is an ongoing challenge.

This interaction between fog and E_z presents an intriguing area of exploration. Investigations into the electrical properties of fog contribute not only to our fundamental understanding of atmospheric phenomena but also have practical implications. These include fog harvesting and dissipation techniques, understanding the influence of aerosols and dust on the atmospheric electric field, and shedding light on the mechanisms underlying solar-terrestrial relationships (Bennett and Harrison, 2008; Giles Harrison and Usoskin, 2010; Guo and Xue, 2021; Khain et al., 2004; Li et al., 2022; Sharifvaghefi and Kazerooni, 2021; Zhang et al., 2023). Furthermore, examining the electrical properties of fog can provide valuable insights for developing models that take into account the microphysics of particle charging and the presence of external ionization and electric field sources in the atmosphere (Guo and Xue, 2021; Sharifvaghefi and Kazerooni, 2021).

Measurements of the atmospheric electric field in arid, desert regions are scarce in comparison to those in wetter or mid-latitude regions. To the author's knowledge, vertical electric field measurements over the UAE were only made at Al Ain, in eastern UAE, and were used to study the effect of sea breeze (Nicoll et al., 2020, 2022). Nicoll et al. (2020) reported a drop of around 7 kV m^{-1} in the electric field when the sea-breeze reached Al Ain. This drop in E_z was attributed to the associated vertical mixing. It's important to note that the changes in E_z were predominantly linked to the onset of the sea breeze front rather than the sea breeze itself. The authors also noted that the electric field at the site is negative (i.e. pointing downwards). This is contradictory to the general understanding of static electrical fields during fog and dust events. In such events, positively-charged particles remain closer to the surface while smaller negatively-charged ones are lofted above, leading to an upward pointing E_z. For instance, the electrification of dust-lofting gust fronts in the Sahel has shown the appearance of an electric field pointing downwards (Williams et al., 2009). The observations at Al Ain might include factors like the dust's composition/mineralogy, the size of the particles, and local turbulence playing a role in lifting positively charged particles upwards. In Nicoll et al. (2022), the authors noted that local meteorological and dust processes may overwhelm the signal from the global electrical circuit (GEC) in the variability of E_z. They also highlighted that the desert environment around Al Ain is highly electrified, in particular in the summer period and during daytime.

This work focuses on examining the diurnal variability of E_z in one of the most unique and extreme environments on the planet - the Empty Quarter desert (Rub' al Khali) in the UAE. This region, known for its

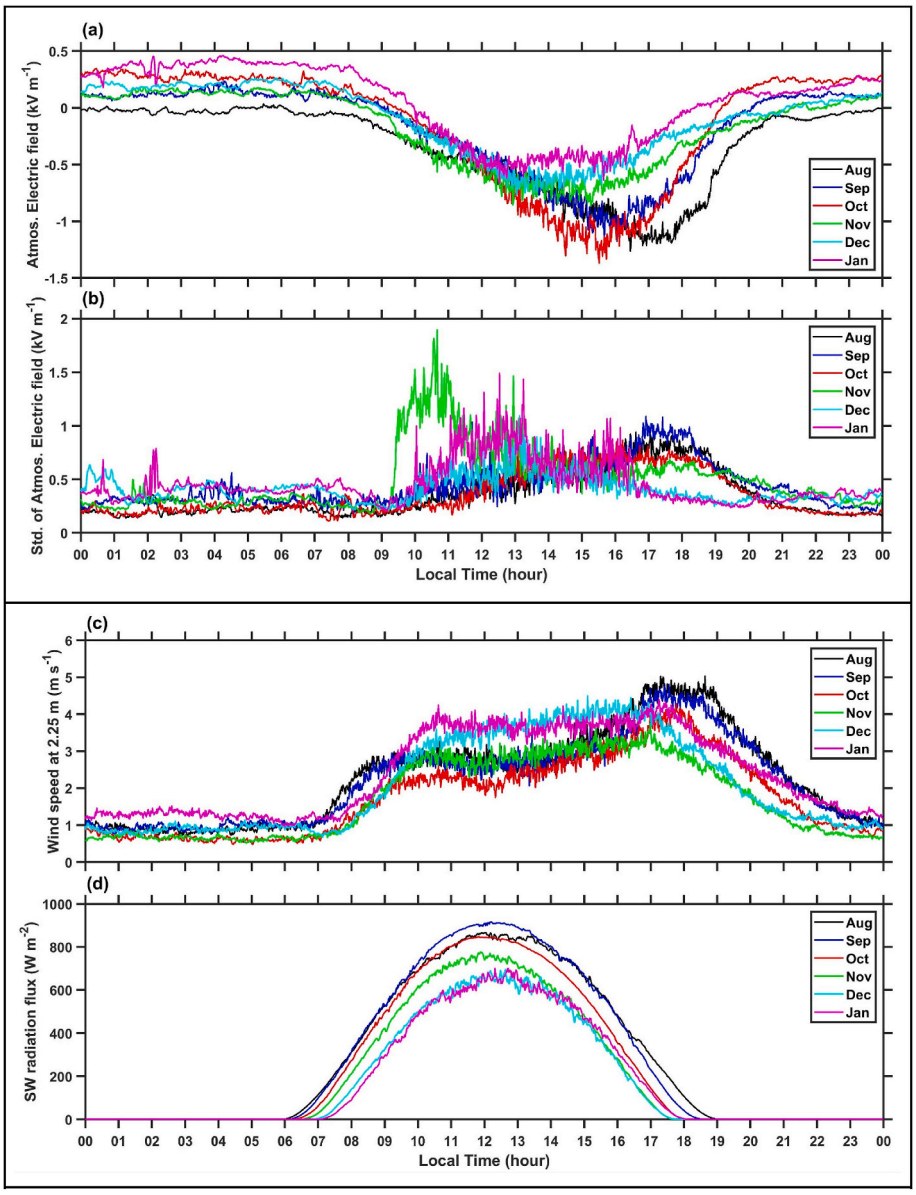

Fig. 1. Diurnal variability in atmospheric electric field: (a) Mean and (b) standard deviation (kV m^{-1}) of the electric field E_z, (c) wind speed (m s^{-1}) at 2.25 m, and (d) Incoming shortwave (SW) radiation flux (W m^{-2}), from August 2022 to January 2023.

intense heat, vast sand dunes, and occasional dust storms, provides a distinctive environment for such studies. Our investigation spans across different seasons and comprises a range of meteorological conditions from windy and dusty days to fog/haze occurrences, seeking to understand how various weather events can potentially affect E_z's behavior. Here, we delve into the relationship between the fog occurrence and its impact on E_z's variability, which can provide valuable insights into the broader dynamics of the Earth's electric field in addition to furthering our knowledge of local atmospheric conditions. In this paper, section 2 describes the instrumentation, data and methodology, section 3 includes a discussion of the results, and section 4 presents a summary of the main findings.

2. Instrumentation, data and methodology

The *Wind-Blown Sand Experiment (WISE)-UAE* experiment was conducted at Madinat Zayed (23.5761° N, 53.7242° E; elevation: 119 m) located 120 km south-west of Abu Dhabi, UAE. The ground surface is flat with a fetch of more than 300-m in the maximum prevailing wind direction. The soil type, loamy sand, is prone to wind erosion. Observations employed during this study include the vertical component of the atmospheric electric field (E_z), measured using a Campbell Scientific electric field mill (CS110); horizontal visibility from the SEN-TRY™ Visibility Sensor 1 (SVS1, Temimi et al., 2020a); meteorological parameters from a 10-m high micrometeorological tower; and aerosol number and mass concentrations from an optical particle counter (OPC, GRIMM 1.108) and nephelometer (DataRAM 4, DR-4000) installed at 2 m above ground level. The OPC measures dust particles in 15 size-classes ranging from 0.3 to 20 μm (namely 0.3–0.4, 0.4–0.5, etc., Sow et al., 2009). The nephelometer measures the aerosol mass concentration up to 400 mg m^{-3}. More details on the experiment site description, instrumentation, and background weather conditions prevailing during *WISE-UAE* are detailed in Nelli et al. (2023). In the current study, only E_z data corresponding to a status code of less than 4 is considered. We use the standard physics sign convention in this study: $E_z > 0$ means a positive test charge would move upward. Measurements were taken at 1 Hz, and 1-min averages and standard deviations were calculated to study diurnal variations and the impact of fog on E_z variability.

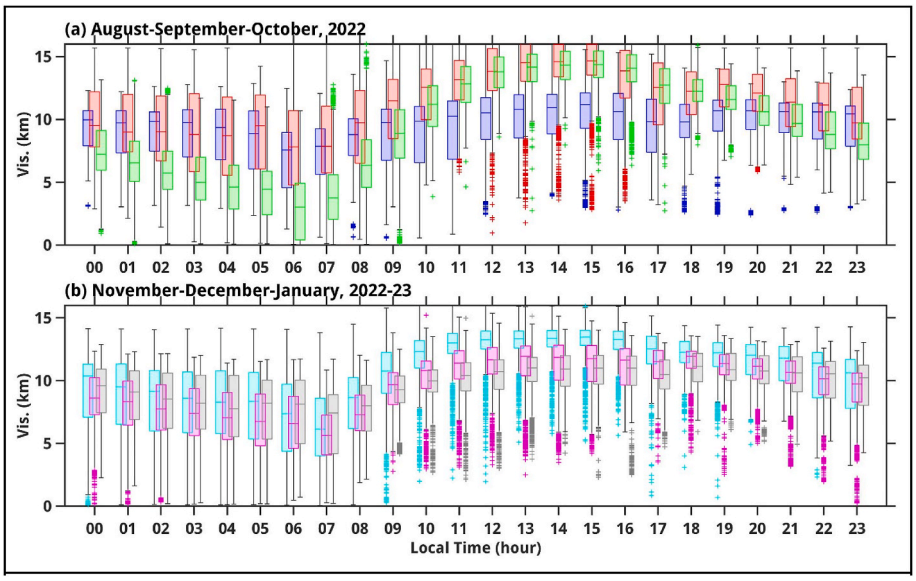

Fig. 2. Box plot of the horizontal visibility in diurnal scale for the months August 2022 to January 2023.

Horizontal visibility, meteorological variables, and aerosol concentrations are measured every minute. Stringent quality checks on meteorological tower data are applied as described in Reddy and Rao (2018). The above-mentioned data is analyzed for *WISE-UAE* Phase-1 period, which spanned from 25 July 2022 to 07 February 2023, to quantify the impact of foggy conditions on the measured electric field. We gain insight into the fog's spatial extent by analyzing false-color red--green-blue (RGB) satellite images from the Spinning Enhanced Visible and Infrared Imager (SEVIRI) on the Meteosat Second Generation spacecraft (Weston et al., 2021; Nelli et al., 2022). These RGB images are updated every 15 min and offer a spatial resolution of approximately 5.6 km (0.05° × 0.05°), covering the geographic bounds of 60°S–60°N and 60°W–60°E. For atmospheric field data, we utilized the European Center for Medium Range Weather Forecasting's (ECMWF) ERA-5 reanalysis datasets, as detailed in Hersbach et al. (2018a, 2018b, 2019a, 2019b).

In this study, fog cases are detected using horizontal visibility measurements, relative humidity (RH, 2-m height), and wind speed (2.25 m and 10-m heights). Initially, fog is detected subject that the horizontal visibility is less than or equal to 1 km, and that RH is greater than 90% (Temimi et al., 2020a; Mohan et al., 2020; Weston et al., 2022; Nelli et al., 2022; Fonseca et al., 2023). Subsequently, a visual inspection of 15-min SEVIRI Fog RGB images is conducted to confirm the presence of fog at the detected times (Weston et al., 2021; Nelli et al., 2022). Furthermore, cloudy or rainy conditions are filtered out using the 30-min merged Infrared brightness temperature (IRBT) data from geostationary satellites averaged around the *WISE-UAE* location (Rao et al., 2013; Reddy and Rao, 2018; Subrahmanyam et al., 2020; Nelli et al., 2021b), and the radar precipitation sensor installed at 10-m height. Throughout the observed period, a total of 27 fog events were recorded, each varying in duration from 17 min to approximately 8 h and 41 min (Nelli et al., 2023). The duration considered here is the sum of the time stamps from fog onset to its complete dissipation. Note that for some cases, the visibility is above 1 km in between (fog-haze-fog) fog onset and complete dissipation. These time intervals are excluded from the fog duration calculation. Electric field data for 18 October 2022 is not available due to data transmission issues. The average wind speed during fog events was 0.9 ± 0.4 m s^{-1}. The longest-lasting fog event occurred on 13 November 2022. All times are local time (UTC+4) unless otherwise stated.

3. Results

The atmospheric vertical electric field is not immune to the influences of various weather events, including but not limited to, fog, convective systems, and dust storms. Under typical fair-weather conditions, the electric field at the site generally points downward (negative E_z, using the customary sign convention from physics) in line with the findings of Nicoll et al. (2020). Its diurnal variations can be significantly perturbed in response to different weather events, seasonal changes, and geographical influences (Yaniv et al., 2016). Below we present the diurnal variability in E_z during different seasons.

3.1. Diurnal variability in atmospheric electric field

Fig. 1 illustrates the diurnal cycle of E_z (mean and standard deviation depicted in 1a-b), wind speed at 2.25 m, and shortwave radiation flux (SW) from August 2022 to January 2023. Due to limited data availability of less than seven days, the months of July 2022 and February 2023 are excluded. A box plot representing the diurnal variation of horizontal visibility from August 2022 to January 2023 is presented in Fig. 2. The diurnal variability of E_z is given by the Carnegie curve (Harrison, 2013), with a maximum around 19 UTC (23 local time, LT) and a minimum around 03 UTC (07 LT). Our observations show a markedly different variability, with a minimum around 13 and 18 LT in all months. At locations in desert areas, such as WISE-UAE, electric field data can deviate from the Carnegie Curve due to the influence of dust load, which reduces the air conductivity. This is in line with the findings of Nicoll et al. (2022) who noted that at Al Ain the diurnal variability of E_z is mostly governed by local, rather than global, processes. The earlier occurrence of the minimum from summer to winter is consistent with Harrison (2013) observations and may also arise from an earlier onset of the sea breeze (Eager et al., 2008). The diurnal minimum of E_z varies between −0.5 and −1.4 kV m^{-1} across different months: 1.2 kV m^{-1} in August, −1.1 kV m^{-1} in September, −1.4 kV m^{-1} in October, −0.7 kV m^{-1} in November, −0.6 kV m^{-1} in December, and −0.5 kV m^{-1} in January. The amplitude of this diurnal minimum appears to be significantly influenced by the diurnal maxima of both wind speed and incoming shortwave radiation flux (as depicted in Fig. 1c–d).

Our findings demonstrate a strong negative correlation between the diurnal fluctuations of E_z and surface wind speed, with a 99% confidence level. The correlation coefficient ranges from −0.763 in September to −0.952 in December, with this relationship attributed to several

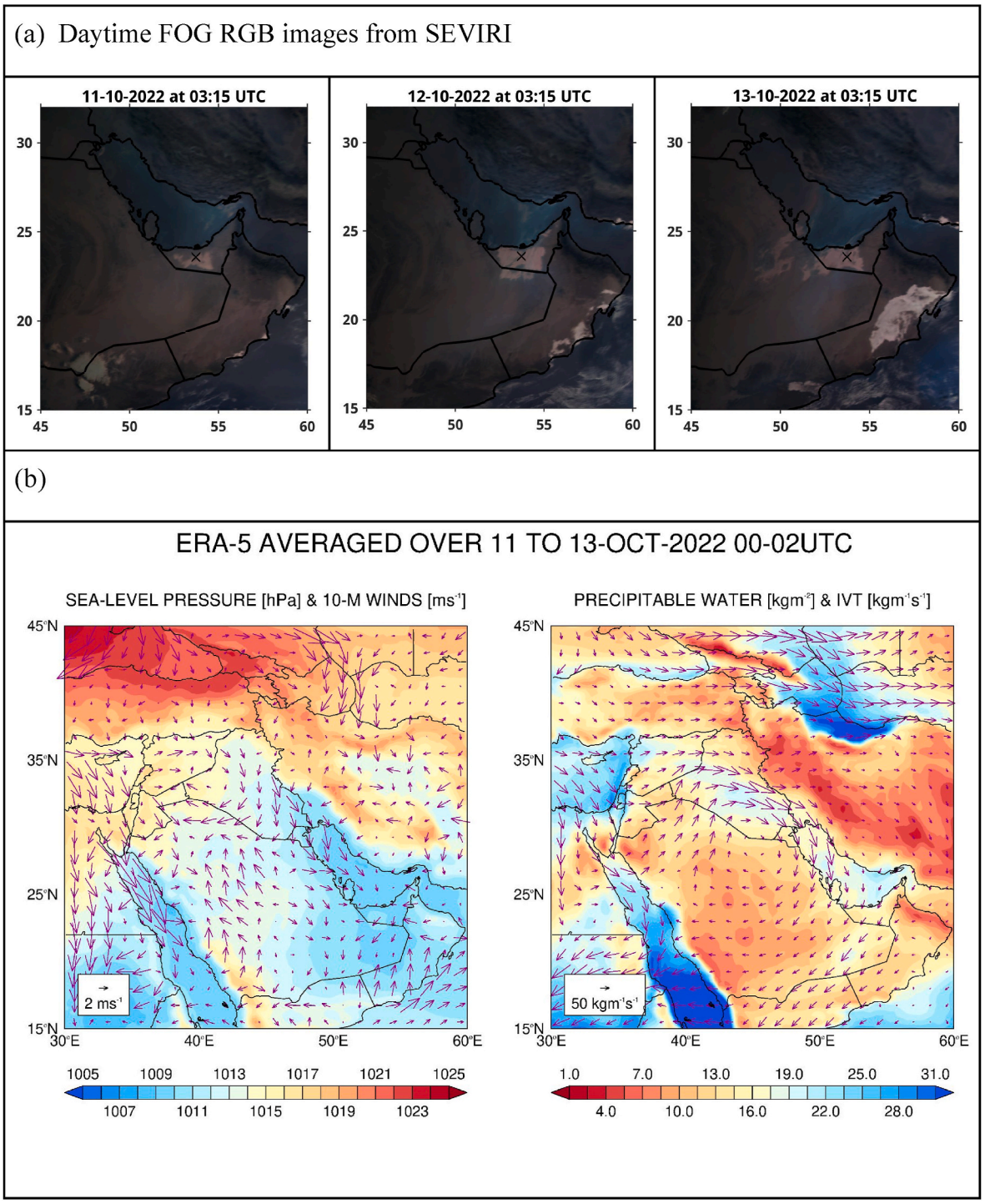

Fig. 3. Meteorological conditions during the 11–13 October 2022 fog events (a) Fog red-green-blue (RGB) composite images from SEVIRI for the 11 to 13 of October 2022 at 03:15 UTC (07:15 LT). The 'x' mark denotes the location of the WISE-UAE experiment. ERA-5 fields averaged over 11 to 13 of October 2022 for 00–02 UTC: sea-level pressure (shading; hPa) and 10-m wind vectors (arrows; m s^{-1}) (left), and precipitable water (shading; kg m^{-2}) and integrated vapor transport (arrows; kg m^{-1} s^{-1}) (right). (b) Actual and (c) Anomalies.

physical phenomena. High wind speeds can cause dust and other soil particles to become airborne. These airborne particles, which often carry electric charges, can redistribute them within the atmosphere due to wind-induced movement, thereby influencing E_z. Frictional or tribo-electric charging, a process in which materials acquire electric charge through frictional contact with other materials, is another contributing factor. In high wind conditions, air laden with dust particles moving against the Earth's surface can lead to the charging of these particles, with the subsequent movement and interaction with each other affecting the electric field. In a desert environment, high wind speeds often initiate a process known as saltation, wherein sand particles are lifted from the ground and bounce along the surface. This process can result in the triboelectric charging of sand particles, further influencing E_z. In all these scenarios, the lighter negatively charged particles and their

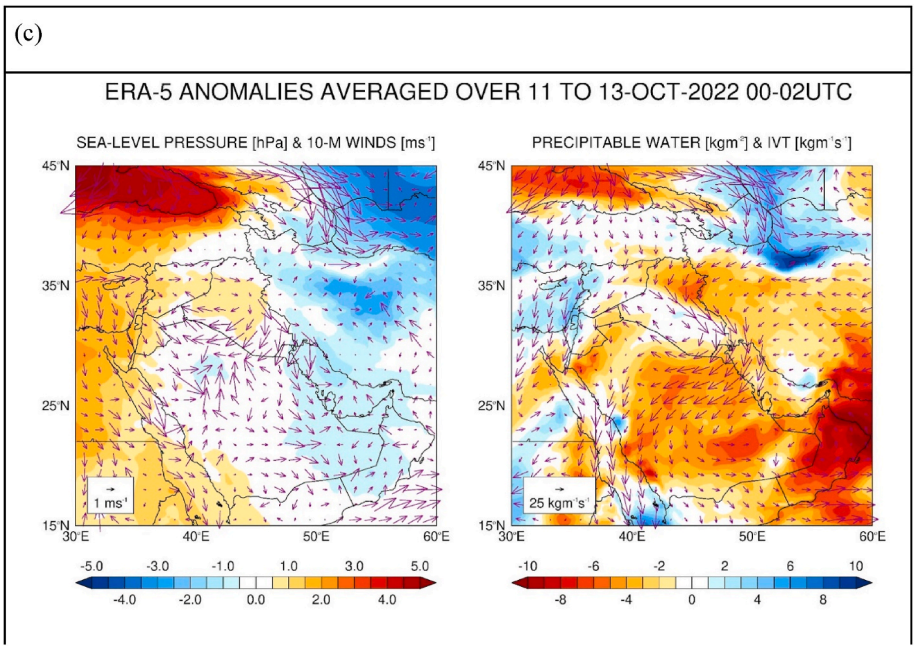

Fig. 3. (*continued*).

movement within the atmosphere can amplify the downward (negative) direction of E_z. Thus, E_z becomes more negative (higher in magnitude) with increased wind speed. The drop in magnitude and the increase in the variability of E_z during daytime, as seen by comparing Fig. 1a–b with 1d, is consistent with the more unstable daytime boundary layer and enhanced vertical mixing as evidenced by the higher wind speeds (Fig. 1c).

Understanding the interactions between atmospheric electricity and meteorological conditions is instrumental in advancing our knowledge of weather dynamics and atmospheric electricity. The noticeably high standard deviation of E_z observed from 9 to 12 LT during November can be attributed to two main factors: extended fog or haze conditions (Fig. 4), and the occurrence of intense saltation driven by intermittent strong wind conditions. Despite the fact that the monthly average wind speed during those hours is among the lowest for all six months (Fig. 1c), the visibility shows a pronounced variability at that time that exceeds that in all other months (Fig. 2), reflecting the higher fog/haze and saltation occurrences. These weather events can significantly modify the local electric field by altering the vertical distribution of atmospheric ions and charging sand particles. The intricate correlation between E_z, wind, and saltation will be the subject of a subsequent article. In this study, the complex relationship between E_z and conditions of high relative humidity or fog will be expounded in the following section.

3.2. *Impact of fog occurrence on atmospheric electric field*

To assess the impact of fog on the vertical electric field, we selected a case study featuring consecutive foggy days with varying durations from the 11 to 13 October 2022. Instantaneous daytime Fog red-green-blue (RGB) composite images for these three foggy days at 03:15 UTC (07:15 LT) from SEVIRI are presented in Fig. 3a. In order to investigate the synoptic conditions during these foggy days, we used ERA-5 products, which are shown in Fig. 3b–c. Fig. 4 show the time series of the vertical electric field, relative humidity, horizontal visibility, 10-m wind speed and wind direction. The spatial extent and intensity of fog on the 12 and 13 of October 2022 are nearly identical as seen in Fig. 3a. However, the duration of fog at the *WISE-UAE* location for the fog event on 13 October 2022 is nearly twice of that on 12 October (04:19 h vs. 02:16 h, Fig. 4a).

An analysis of the large-scale circulation pattern, as given by ERA-5 reanalysis data, at the time of the three fog events, indicates the following features: (i) high pressure over western Asia to the north of 35° N and the eastern Mediterranean with lower pressure system over the Arabian Peninsula; (ii) a flow of moisture from the Red Sea and the Mediterranean Sea, important moisture sources for the UAE (Nelli et al., 2021a), into the Arabian Gulf and subsequently into the UAE; (iii) weak wind speeds over the country, mostly from an offshore direction, which, together with the more moist air coming from the Arabian Gulf, promote the development of fog. This is the typical atmospheric circulation setup prone to fog occurrence in the UAE (e.g. Mohan et al., 2020; Fonseca et al., 2023).

The spatial extent of the fog on the 12 and 13 of October 2022 was similar, as depicted in Fig. 3a. Notably, the sea breeze was stronger on 12 October, which was followed by an extended period of weak wind conditions (Fig. 4b). This could have potentially contributed to a longer duration of fog occurrence on 13 October (Fig. 4a). More detailed analysis and discussion on the large-scale circulation patterns occurring during consecutive fog events in the UAE can be found in Fonseca et al. (2023).

Fig. 4a illustrates the observed E_z values during the fog events on 11, 12, and 13 October 2022. It is evident from Fig. 4a that the E_z values are higher during the fog event on 13 October compared to those on 11 and 12 October. This observation is notable, considering the similar intensity and spatial extent of these fog events. It suggests that other factors, such as distribution of particles and the duration of the fog, might play significant roles in modulating E_z. The maximum and minimum E_z values measured during the fog event on 13 October are 1.783 kV m^{-1} and -0.781 kV m^{-1}, respectively. It's important to note that E_z returned to background values before the fog lifted. In order to investigate the potential impact of the particle number and mass concentration on E_z, the total particle number concentration (0.3–20 μm) from the Optical Particle Counter (OPC), the mass concentrations from the dust profiler and DataRam, and the particle size distribution from the OPC are analyzed (Fig. 5a–b). Upon the onset of the fog, a notable increase in particle number concentration can be observed (Fig. 5a), while a reduction in the number concentration during the mature and dissipation stages is likely associated with the effects of wet scavenging. The wind speed on 12 October exhibits two distinct peaks around 10 LT and 17 LT, accompanied by prolonged saltation events (Fig. 4b).

This pattern contrasts with that of 11 October, where the wind speed

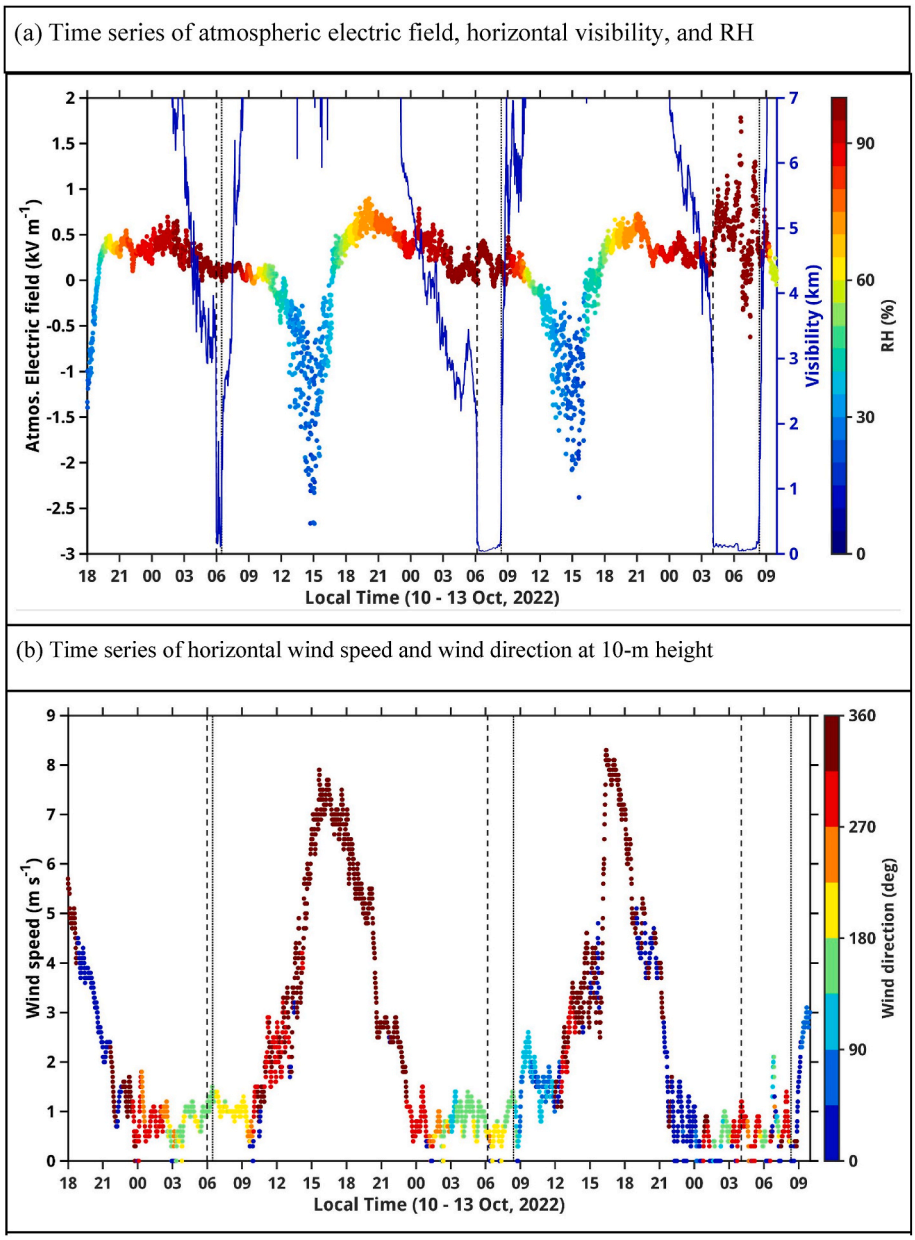

Fig. 4. (a–b) Time series of atmospheric electric field E_z (kV m^{-1}), horizontal visibility (km), relative humidity (RH; %), horizontal wind speed (m s^{-1}) and wind direction (°) from the 10 to 13 of October 2022. RH and wind direction are shaded. The vertical lines in panels a and b indicate the onset (dotted line) and the complete dissipation (dotted line) of the fog.

does not peak around 10 UTC and the duration of saltation is shorter. Interestingly, the peaks in wind speed appear to correlate well with the peaks in both number and mass concentration (Figs. 4b and 5a). Furthermore, the background particle number concentration on the foggy day of 12 October is higher than that of 13 October. Of particular note is the higher concentration of fine particles (<4 μm) on 12 October (Fig. 5b). Fine particles in the atmosphere can significantly influence E_z due to their ability to carry and redistribute electric charges. Given their large surface area to volume ratio, fine particles can hold more electric charges per unit mass compared to larger particles. A decrease in fine particle concentration, as seen from 12 to 13 of October, reduces the total charge density in the atmosphere, potentially leading to an increase in E_z due to the reduced availability of charge carriers (Fig. 5b). This can potentially account for the maximum variability in the electric field observed on 13 October. Moreover, the mobility of charged particles, which depends on particle size, also influences E_z. Smaller particles are more mobile and can be transported more easily by wind flow and turbulence, thereby affecting the distribution of electric charges in the atmosphere and subsequently the electric field (Piper and Bennett, 2012). Normalized mass distribution for all fog events is shown in Fig. 5c. Note that the mass of fine particles decreases while that of coarse particles increases upon the onset of the fog. However, it is understood that within this specific size range (Fig. 5b–c), all particles are susceptible to transportation by wind and turbulence elements, contributing to the variability in the atmospheric electric field (Webb et al., 2021).

Next, we present the electric field variability for 26 distinct fog events that took place during our analysis period, excluding the event on 18 October 2022 due to unavailable E_z data. The actual variations in E_z measurements from the onset of the fog to the complete dissipation for 26 fog events is shown as boxplot in Fig. 6a. Animation of time series of E_z, horizontal visibility, and relative humidity for all fog cases is given in Fig. S1. The horizontal visibility variations are shown as a box plot in Fig. 6b, considering 1 h before the fog's onset, in order to examine whether the onset is gradual or sudden; during the fog; 15 min after its

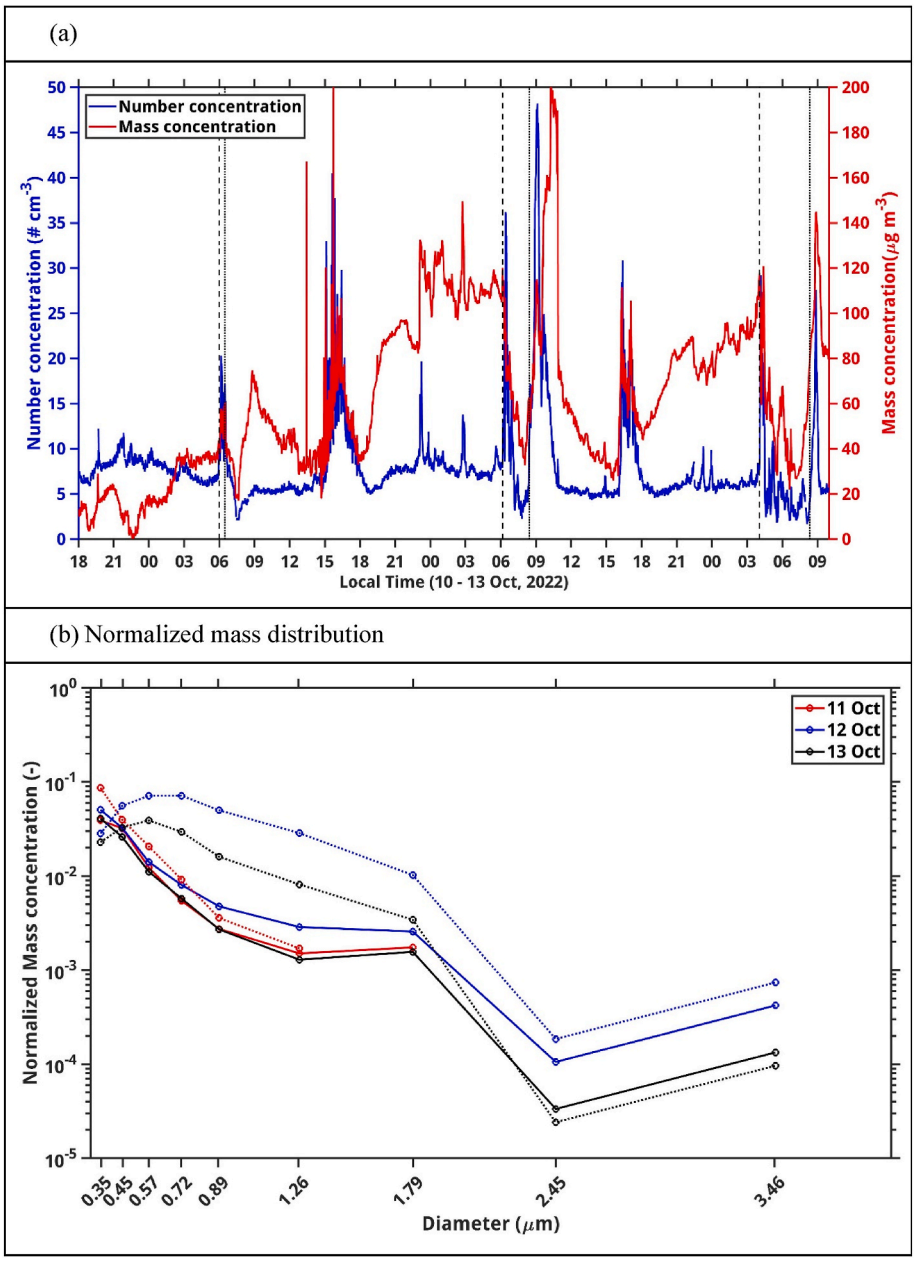

Fig. 5. Particle size distribution during the 11–13 October 2022 fog events (a) Time series of the total particle number concentration (0.3–20 μm; # cm^{-3}) from the OPC (blue line) and mass concentration (μg m^{-3}) from DataRam4 (Red line) at 2-m height, and (b) Normalized mass concentration distribution from the OPC for the three consecutive fog cases. Solid (dotted) lines indicate the average mass distribution 1 h before (during) the fog occurrence. (c) Normalized mass size distribution for all fog events.

dissipation, so as to observe the lifting of the fog. This approach was determined after a visual inspection of all 26 fog cases, allowing for a detailed understanding of the fog's electrical properties (Fig. S1). The specific time frames were selected to capture essential transitional stages, which may offer additional insights into the fog's electrical properties, as seen in Fig. S1.

Next, we evaluated the variability of the electric field during fog events with different durations by calculating the difference between the maximum and minimum electric field anomalies. These anomalies were computed by subtracting the respective monthly mean diurnal E_z values from the observed E_z measurements. Notably, days featuring fog events were excluded from this calculation to create a baseline that represents typical atmospheric conditions without fog interference. The estimated electric field variabilities for these 26 fog events are depicted in Fig. 6c. Each bubble represents a unique fog event, with the size of the bubble corresponding to the event's duration, providing a clear visualization of the relationship between fog duration and electric field variability. Notable observations can be made; for instance, the longest fog event recorded during our study occurred on 13 of November 2022, lasting approximately 8 h 41 min, with this event coinciding with the highest observed variability in E_z, peaking at nearly 3.407 kV m^{-1}. Conversely, the shortest fog event, which lasted merely 17 min, took place on 26 November 2022, for which the electric field variability was minimal, barely reaching 0.1 kV m^{-1}.

In our analysis of the relationship between the variability of the electrical field and the duration of fog events, we found a correlation coefficient of 0.828. This indicates a strong positive linear relationship between the two variables (Fig. 7). It is important to emphasize that this

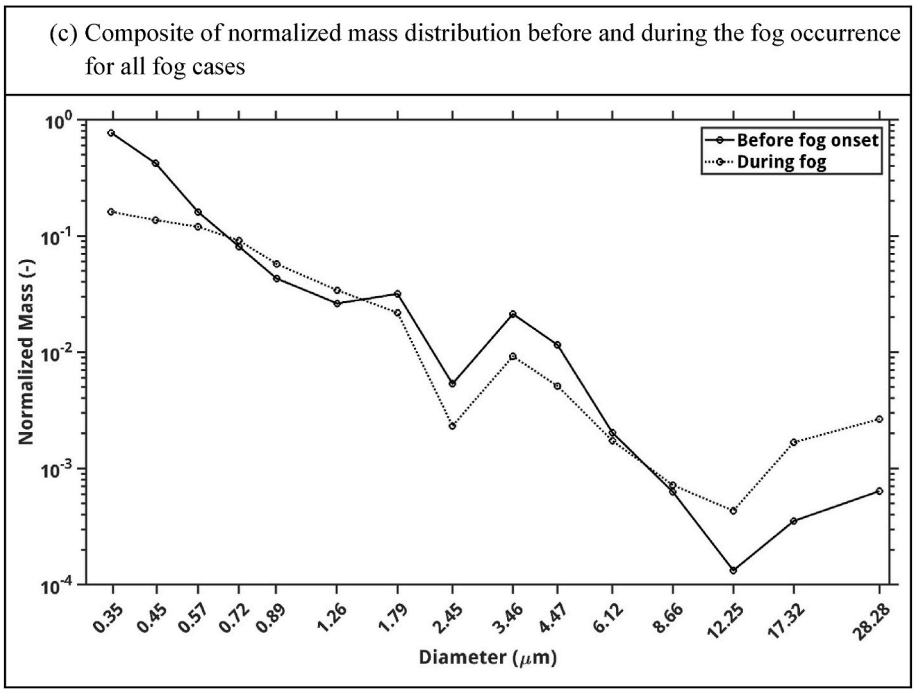

Fig. 5. (*continued*).

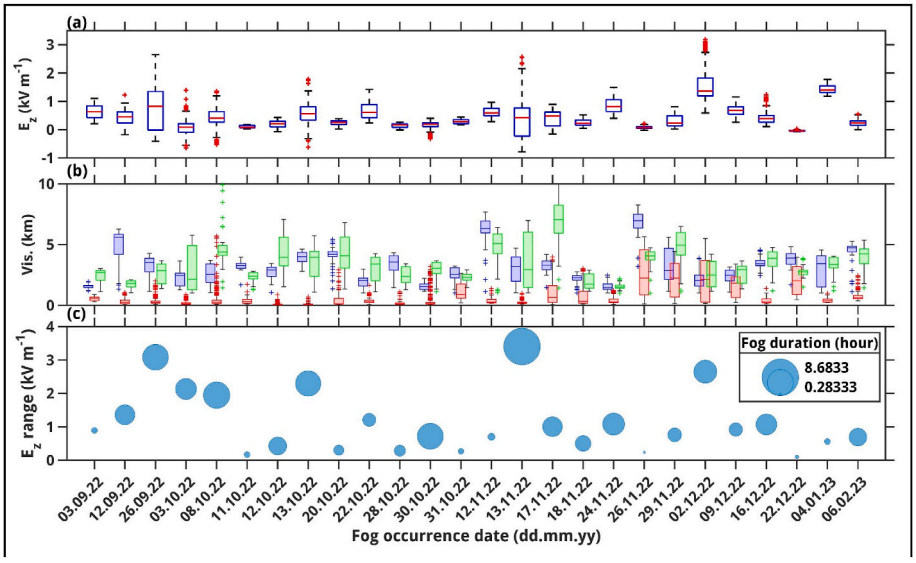

Fig. 6. Statistics of all fog events: (a) Boxplot of the vertical electric field (E_z; kV m^{-1}) measurements from the onset of the fog to the complete dissipation for the 26 fog events. (b) Box plot of horizontal visibility (km) 1 h before (blue box), during (red box), and 15 min after the dissipation of the fog (green box). (c) Variability of E_z anomalies (kV m^{-1}) during the occurrence of the 26 fog events. The size of the bubbles corresponds to the duration of each fog event.

correlation is statistically significant at the 99% confidence level, as evidenced by the confidence interval for the correlation coefficient, which lies between 0.568 and 0.938. Such findings suggest that the duration of fog events has an impact on observed changes in atmospheric electric field variability. This highlights the potential influence and interplay between atmospheric electric fields and foggy conditions in the United Arab Emirates.

In general, the median electric field for fog events is higher and positive (pointing upward), except for four cases (3, 11 October 2022; 26 November 2022; 22 December 2022), which have E_z values less than 0.1 kV m^{-1}. Two factors contribute to this atypical behavior of E_z: first, the change in visibility from haze to fog is gradual, as illustrated in Fig. 4b; second, these instances are very short-duration fog events occurring within haze conditions, as shown in Fig. 6b. These observations underline the combined effects of horizontal visibility changes during the haze-to-fog transition and the duration of fog occurrence in modifying the atmospheric electric field. The interplay between the persistence of the fog and the transition from haze to fog appears to have a pronounced impact on the anomalies in the electric field, suggesting a significant and multifaceted influence of these factors on atmospheric electrical phenomena.

Anisimov et al. (2005) documented six instances of fog at the Borok Observatory in western Russia, demonstrating that the potential gradient (PG) values escalated during fog occurrences up to 350 V m^{-1} while slightly diminishing the atmospheric current density values. Bennett and Harrison (2009) identified an elevation in the PG ranging

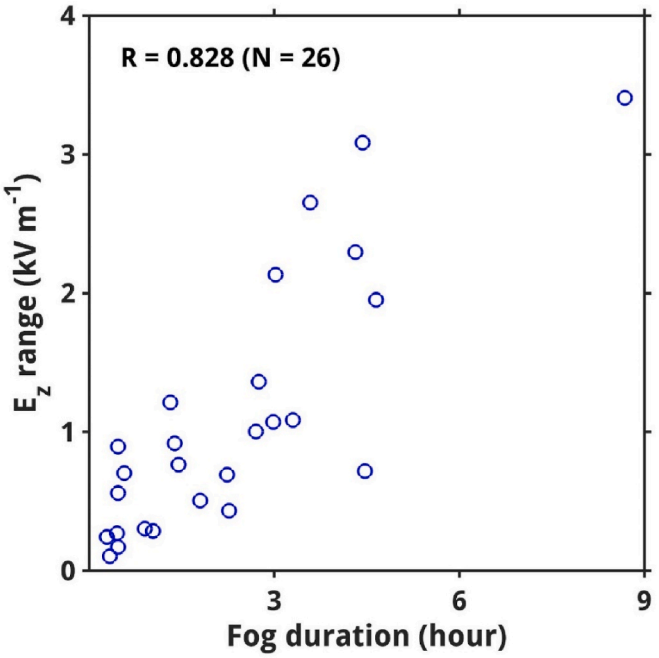

Fig. 7. Scattered plot of Fog duration (hour) versus E_z variability (kV m^{-1}).

between 300 and 800 V m^{-1} at Reading (southern UK) during exceptionally foggy conditions in December 2016, a change that was contingent upon the thickness of the fog (droplet size), although the current density values remained constant. Harrison (2011) observed a twofold increase in the PG measured in Reading during fog conditions, escalating from a median value of 80.6 V m^{-1} to 170.6 V m^{-1}, based on 139 h of data collection. Similarly, (Lucas et al., 2017) recorded an enhancement in the PG of +150 V m^{-1} at sunrise with low wind speeds and high relative humidity conditions at Kennedy Space Center in Florida. More recently, (Yair and Yaniv, 2023) reported the increase in the electric field (up to 400–650 V m^{-1}) compared with the mean fair weather values observed at Negev Desert Highland site in southern Israel. In the present study, the maximum electric field observed for a long-lasting fog event (8 h and 41 min) on 13 November 2022, was 2571 V m^{-1} (Fig. 4a). The median E_z for fog events with duration more than 1 h is 444 V m^{-1}.

In the manuscript, we hypothesize that the notably high E_z values observed in the UAE are attributable to the presence of dust aerosols in this hyper-arid desert region, aligning with existing studies that have reported higher electric field values in dusty environments compared to non-dusty ones (Sow et al., 2011; Nicoll et al., 2020, 2022). However, we acknowledge that this assertion requires further detailed investigation to fully substantiate and understand the mechanisms involved in these elevated E_z values in dusty conditions.

4. Summary

The *Wind-Blown Sand Experiment - United Arab Emirates* (*WISE-UAE)* Phase-1 campaign started on 22 July 2022 at Madinat Zayed, a location approximately 120 km southwest of Abu Dhabi in the Rub' Al Khali desert. During the campaign, 27 fog events with different durations and intensities occurred. In this study, we investigate the impact of the fog events on the atmospheric electric field (E_z). A record high E_z value of 2571 V m^{-1} was measured for a long-lasting fog event (8 h and 41 min) on 13 November 2022. The median E_z for fog events lasting more than 1 h is 444 V m^{-1}.

The higher E_z values, compared to previous studies which report values in the range 80–800 V m^{-1}, are attributable to the dust aerosols present in this hyper-arid desert region. Our observations showed that the longer the fog's duration, the higher the variability in E_z, with an amplitude range of E_z anomalies for long-lasting fog events reaching 3.407 kV m^{-1}. This is primarily because fog acts as an efficient medium for absorbing and redistributing atmospheric electric charges, thereby altering the ion balance and affecting the electrical conductivity and ion mobility within the atmosphere. The more prolonged the fog, the more time available for these interactions, leading to more extensive variations in the atmospheric electric field and resulting in greater variability.

Our results can be applied to develop techniques for fog harvesting and to improve fog forecasting by accounting for the effect of the electric field on fog lifetime and characteristics.

CRediT authorship contribution statement

Narendra Nelli: Conceptualization; Data acquisition and analysis; Interpretation of the results; Writing the original draft; revise the manuscript. **Diana Francis:** Conceptualization, formal analysis; Interpretation of the results; inputs to the manuscripts and review, supervision and fund acquisition. **Ricardo Fonseca:** formal analysis, Interpretation of the results; inputs to the manuscripts and review. **Olivier Masson:** Interpretation of the results; inputs to the manuscripts and review. **Mamadou Sow:** Interpretation of the results; inputs to the manuscripts and review. **Emmanuel Bosc:** Project management and validation of results.

Declaration of competing interest

The authors declare that they have no known competing financial interests or personal relationships that could have appeared to influence the work reported in this paper.

Data availability

Data will be made available on request.

Acknowledgments

The authors wish to acknowledge the contribution of Khalifa University's high-performance computing and research computing facilities to the results of this research. We are also grateful to the SHAMS power company (https://www.shamspower.ae/) and Emirates Tech (ETECH; https://www.etechuae.com/) for their invaluable support and assistance in the deployment of the instruments during the WISE-UAE. This research work was supported by Federal Authority for Nuclear Regulation through the research project Modeling of Radionuclides Dispersion in the UAE Environment (MORAD).

We are grateful to the IRSN for providing Aerosol analyzers, analyzers sample heads. It is with great gratitude that we thank Amel Kort and Pauline Wiszniowski from IRSN for providing aerosol analyzer calibration reports. We would also like to thank an anonymous reviewer for his/her constructive and insightful comments that helped to significantly improve the quality of this work.

Appendix A. Supplementary data

Supplementary data to this article can be found online at https://doi.org/10.1016/j.jaridenv.2023.105096.

References

Abida, R., Nelli, N., Francis, D., Masson, O., Fonseca, R., Bosc, E., Temimi, M., 2023. Microphysics of Radiation Fog and Estimation of Fog Deposition Velocity for Atmospheric Dispersion Applications. https://doi.org/10.5194/egusphere-2023-956.

Aldababseh, A., Temimi, M., 2017. Analysis of the long-term variability of poor visibility events in the UAE and the link with climate dynamics. Atmosphere 8 (12), 242. https://doi.org/10.3390/atmos8120242.

Ambaum, M.H.P., Auerswald, T., Eaves, R., Harrison, R.G., 2022. Enhanced attraction between drops carrying fluctuating charge distributions. Proc. R. Soc. A 478 (2257). https://doi.org/10.1098/rspa.2021.0714.

Anisimov, S.V., Mareev, E.A., Shikhova, N.M., Sorokin, A.E., Dmitriev, E.M., 2005. On the electro–dynamical characteristics of the fog. Atmos. Res. 76 (1–4), 16–28. https://doi.org/10.1016/j.atmosres.2004.11.026.

Bennett, A.J., Harrison, R.G., 2008. Variability in surface atmospheric electric field measurements. J. Phys. Conf. 142, 012046 https://doi.org/10.1088/1742-6596/142/1/012046.

Bennett, A.J., Harrison, R.G., 2009. Evidence for global circuit current flow through water droplet layers. J. Atmos. Sol. Terr. Phys. 71 (12), 1219–1221. https://doi.org/10.1016/j.jastp.2009.04.011.

Bergot, T., Terradellas, E., Cuxart, J., Mira, A., Leichti, O., Mueller, M., Nielsen, N.W., 2007. Intercomparison of single-column numerical models for the prediction of radiation fog. J. Appl. Meteorol. Climatol. 46, 504–521. https://doi.org/10.1175/JAM2475.1.

Bergot, T., Escobar, J., Masson, V., 2015. Effect of small-scale surface heterogeneities and buildings on radiation fog: large-eddy simulation study at paris-charles de gaulle airport. Q. J. R. Meteorol. Soc. 141, 285–298. https://doi.org/10.1002/qj.2358.

Branch, O., Schwitalla, Thomas, Temimi, Marouane, Fonseca, Ricardo, Nelli, Narendra, Weston, Michael, Milovac, Josipa, Wulfmeyer, Volker, 2021. Seasonal and diurnal performance of daily forecasts with WRF V3.8.1 over the United Arab Emirates. Geosci. Model Dev. (GMD) 14, 1615–1637. https://doi.org/10.5194/gmd-14-1615-2021, 2021.

de Villiers, M.P., van Heerden, J., 2007. Fog at Abu Dhabi international airport. Weather 62, 209–214. https://doi.org/10.1002/wea.45.

Eager, R.E., Raman, S., Wootten, A., Westphal, D.K., Reid, J.S., Al Mandoos, A., 2008. A climatological study of the sea and land breezes in the Arabian Gulf region. J. Geophys. Res. 113, D15106 https://doi.org/10.1029/2007JD009710.

Esfandiari, N., Rezaei, M., 2022. Automatic detection, classification, and long-term investigation of temporal-spatial changes of atmospheric rivers in the Middle East. Int. J. Climatol. 42, 7730–7750. https://doi.org/10.1002/joc.7674.

Fonseca, R., Francis, D., Nelli, N., Cherif, C., 2023. Regional atmospheric circulation patterns driving consecutive fog events in the United Arab Emirates. Atmos. Res. 282, 106506 https://doi.org/10.1016/j.atmosres.2022.106506.

Francis, D., Fonseca, R., Nelli, N., Bozkurt, D., Picard, G., Guan, B., 2022. Atmospheric rivers drive exceptional Saharan dust transport towards Europe. Atmos. Res. 266, 105959.

Giles Harrison, R., Usoskin, I., 2010. Solar modulation in surface atmospheric electricity. J. Atmos. Sol. Terr. Phys. 72 (2–3), 176–182. https://doi.org/10.1016/j.jastp.2009.11.006.

Gultepe, I., Milbrandt, J.A., 2007. Microphysical observations and mesoscale model simulation of warm fog case during FRAM project. Pure Appl. Geophys. 164, 1161–1178. https://doi.org/10.1007/s00024-007-0212-9.

Gultepe, I., Pearson, G., Milbrandt, J.A., Hansen, B., Platnick, S., Taylor, P., Gordon, M., Oakley, J.P., Cober, S.G., 2009. The fog remote sensing and modeling field project. Bull. Am. Meteorol. Soc. 90, 341–359. https://doi.org/10.1175/2008BAMS2354.1.

Guo, S., Xue, H., 2021. The enhancement of droplet collision by electric charges and atmospheric electric fields. Atmos. Chem. Phys. 21 (1), 69–85. https://doi.org/10.5194/acp-21-69-2021.

Harrison, R.G., 2003. Ion-aerosol-cloud processes in the lower atmosphere. Rev. Geophys. 41 (3), 1012. https://doi.org/10.1029/2002RG000114.

Harrison, R.G., 2011. Fair weather atmospheric electricity. J. Phys. Conf. 301, 012001 https://doi.org/10.1088/1742-6596/301/1/012001.

Harrison, R. Giles, 2013. The Carnegie curve. Surv. Geophys. 34 (2), 209–232. https://doi.org/10.1007/s10712-012-9210-2.

Hersbach, H., Bell, B., Berrisford, P., Biavati, G., Horanyi, A., Munoz Sabater, J., et al., 2018a. ERA5 Hourly Data on Pressure Levels from 1979 to Present. *Copernicus Climate Change Service (C3S) Climate Data Store (CDS)*. https://doi.org/10.24381/cds.bd0915c6.

Hersbach, H., Bell, B., Berrisford, P., Biavati, G., Horanyi, A., Munoz Sabater, J., et al., 2018b. ERA5 Hourly Data on Single Levels from 1979 to Present. *Copernicus Climate Change Service (C3S) Climate Data Store (CDS)*. https://doi.org/10.24381/cds.adbb2d47.

Hersbach, H., Bell, B., Berrisford, P., Biavati, G., Horanyi, A., Munoz Sabater, J., et al., 2019a. ERA5 Monthly Averaged Data on Pressure Levels from 1979 to Present. Copernicus Climate Change Service (C3S) Climate Data Store (CDS). https://doi.org/10.24381/cds.6860a573.

Hersbach, H., Bell, B., Berrisford, P., Biavati, G., Horanyi, A., Munoz Sabater, J., et al., 2019b. ERA5 Monthly Averaged Data on Single Levels from 1979 to Present. *Copernicus Climate Change Service (C3S) Climate Data Store (CDS)*. https://doi.org/10.24381/cds.f17050d7.

Jia, X., Quan, J., Zheng, Z., Liu, X., Liu, Q., He, H., Liu, Y., 2019. Impacts of anthropogenic aerosols on fog in north China plain. J. Geophys. Res. Atmos. 124 (1), 252–265. https://doi.org/10.1029/2018JD029437.

Khain, A., Arkhipov, V., Pinsky, M., Feldman, Y., Ryabov, Y., 2004. Rain enhancement and fog elimination by seeding with charged droplets. Part I: theory and numerical simulations. J. Appl. Meteorol. 43 (10), 1513–1529. https://doi.org/10.1175/JAM2131.1.

Li, D., Li, C., Li, J., Yang, W., Xiao, M., Zhang, M., et al., 2022. Efficient corona discharge fog collector: multiple mesh electrodes with electric field enhances fog harvesting. Plasma Chem. Plasma Process. 42 (6), 1249–1264. https://doi.org/10.1007/s11090-022-10279-7.

Lucas, G.M., Thayer, J.P., Deierling, W., 2017. Statistical analysis of spatial and temporal variations in atmospheric electric fields from a regional array of field mills. J. Geophys. Res. Atmos. 122 (2), 1158–1174. https://doi.org/10.1002/2016JD025944.

Massoud, E., Massoud, T., Guan, B., Sengupta, A., Espinoza, V., De Luna, M., Raymond, C., Waliser, D., 2020. Atmospheric rivers and precipitation in the Middle East and north africa (MENA). Water 12, 2863. https://doi.org/10.3390/w12102863.

Mohan, T.S., Temimi, M., Ajayamohan, R.S., Nelli, N.R., Fonseca, R., Weston, M., Valappil, V., 2020. On the investigation of the typology of fog events in an arid environment and the link with climate patterns. Mon. Weather Rev. 148 (8), 3181–3202. https://doi.org/10.1175/MWR-D-20-0073.1.

Nelli, N., Temimi, M., Fonseca, R.M., Weston, M.J., Thota, M.S., Valappil, V.K., Branch, O., Wulfmeyer, W., Wehbe, Y., Al Hosary, T., Shalaby, A., Al Shamsi, N., Al Naqbi, H., 2020. Impact of roughness length on WRF simulated Land-Atmosphere Interactions over a hyper-arid region. J. Earth Space Sci. 7, e2020EA001165 https://doi.org/10.1029/2020EA001165.

Nelli, N., Fissehaye, S., Francis, D., Fonseca, R., Temimi, M., Weston, M., et al., 2021a. Characteristics of atmospheric aerosols over the UAE inferred from CALIPSO and sun photometer aerosol optical depth. Earth Space Sci. 8 (6) https://doi.org/10.1029/2020EA001360.

Nelli, N.R., Francis, D., Fonseca, R., Abida, R., Weston, M., Wehbe, Y., Al Hosary, T., 2021b. The atmospheric controls of extreme convective events over the southern Arabian Peninsula during the spring season. Atmos. Res. 262, 105788 https://doi.org/10.1016/j.atmosres.2021.105788.

Nelli, N., Francis, D., Fonseca, R., Bosc, E., Addad, Y., Temimi, M., et al., 2022. Characterization of the atmospheric circulation near the Empty Quarter Desert during major weather events. Front. Environ. Sci. 10 https://doi.org/10.3389/fenvs.2022.972380.

Nelli, N., Francis, D., Sow, M., Bosc, E., Bergametti, G., 2023. The WInd-Blown Sand Experiment (WISE)–UAE: Introduction and First Results. Copernicus Meetings. https://doi.org/10.5194/egusphere-egu23-3512. EGU23-3512.

Nicoll, K., Harrison, G., Marlton, G., Airey, M., 2020. Consistent dust electrification from Arabian Gulf sea breezes. Environ. Res. Lett. 15 (8), 084050 https://doi.org/10.1088/1748-9326/ab9e20.

Nicoll, K.A., Readle, A., Al Kamali, A., Harrison, R.G., 2022. Surface atmospheric electric field variability at a desert site. J. Atmos. Sol. Terr. Phys. 241, 105977 https://doi.org/10.1016/j.jastp.2022.105977.

Piper, I.M., Bennett, A.J., 2012. Observations of the atmospheric electric field during two case studies of boundary layer processes. Environ. Res. Lett. 7 (1), 014017 https://doi.org/10.1088/1748-9326/7/1/014017.

Rao, K.G., Narendra Reddy, N., Ramakrishna, G., Bhuyan, P.K., Bhuyan, K., Kalita, G., Pathak, B., 2013. Near surface atmospheric response to the total solar eclipse at dibrugarh on 22 July 2009. J. Atmos. Sol. Terr. Phys. 95 (96), 87–95. https://doi.org/10.1016/j.jastp.2013.01.001.

Reddy, N.N., Rao, K.G., 2018. Contrasting variations in the surface layer structure between the convective and non-convective periods in the summer monsoon season for Bangalore location during PRWONAM. J. Atmos. Sol. Terr. Phys. 167, 156–168. https://doi.org/10.1016/j.jastp.2017.11.017.

Sharifvaghefi, S., Kazerooni, H., 2021. Fog harvesting: combination and comparison of different methods to maximize the collection efficiency. SN Appl. Sci. 3 (4), 516. https://doi.org/10.1007/s42452-021-04518-3.

Sow, M., Alfaro, S.C., Rajot, J.L., Marticorena, B., 2009. Size resolved dust emission fluxes measured in Niger during 3 dust storms of the AMMA experiment. Atmos. Chem. Phys. 9 (12), 3881–3891. https://doi.org/10.5194/acp-9-3881-2009.

Sow, M., Crase, E., Rajot, J.L., Sankaran, R.M., Lacks, D.J., 2011. Electrification of particles in dust storms: field measurements during the monsoon period in Niger. Atmos. Res. 102 (3), 343–350. https://doi.org/10.1016/j.atmosres.2011.08.010, 2011.

Stolaki, S.N., Kazadzis, S.A., Foris, D.V., Karacostas, T.S., 2009. Fog characteristics at the airport of Thessaloniki, Greece. Nat. Hazards Earth Syst. Sci. 9, 1541–1549. https://doi.org/10.5194/nhess-9-1541-2009.

Subrahmanyam, K.V., Kumar, K.K., Reddy, N.N., 2020. New insights into the convective system characteristics over the Indian summer monsoon region using space-based Passive and active remote sensing techniques†. IETE Tech. Rev. 37 (2), 211–219. https://doi.org/10.1080/02564602.2019.1593890.

Temimi, M., Fonseca, R.M., Nelli, N.R., Valappil, V.K., Weston, M.J., Thota, M.S., et al., 2020a. On the analysis of ground-based microwave radiometer data during fog conditions. Atmos. Res. 231, 104652 https://doi.org/10.1016/j.atmosres.2019.104652.

Temimi, M., Fonseca, R.M., Nelli, Narendra, Weston, M.J., Thota, M.S., Valappil, V., Branch, O., Wizemann, H.-D., Wehbe, Y., Al Hosary, T., Shalaby, A., Al Shamsi, N., Al Naqbi, H., 2020b. Assessing the impact of changes in land surface conditions on WRF predictions in arid regions. J. Hydrometeorol. 21 (12), 2829–2853. https://doi.org/10.1175/JHM-D-20-0083.1.

Valappil, V.K., Temimi, M., Weston, M., Fonseca, R., Nelli, Narendra, Thota, M., Kumar, K.N., 2019. Assessing bias correction methods in support of operational weather forecast in arid environment. Asia-Pac. J. Atmosp. Sci. 56, 333–347. https://doi.org/10.1007/s13143-019-00139-4.

Verma, S., Ramana, M.V., Kumar, R., 2022. Atmospheric rivers fueling the intensification of fog and haze over Indo-Gangetic Plains. Sci. Rep. 12 (1), 5139. https://doi.org/10.1038/s41598-022-09206-9.

Webb, N.P., LeGrand, S.L., Cooper, B.F., Courtright, E.M., Edwards, B.L., Felt, C., et al., 2021. Size distribution of mineral dust emissions from sparsely vegetated and supply-limited dryland soils. J. Geophys. Res. Atmos. 126, e2021JD035478 https://doi.org/10.1029/2021JD035478.

Westcott, N.E., Kristovich, D.A.R., 2009. A climatology and case study of continental cold season dense fog associated with low clouds. J. Appl. Meteorol. Climatol. 48, 2201–2214. https://doi.org/10.1175/2009JAMC1999.1.

Weston, M., Temimi, M., Fonseca, R.M., Nelli, N.R., Francis, D., Piketh, S., 2021. A rule-based method for diagnosing radiation fog in an arid region from NWP forecasts. J. Hydrol. 597, 126189 https://doi.org/10.1016/j.jhydrol.2021.126189.

Weston, M., Francis, D., Nelli, N., Fonseca, R., Temimi, M., Addad, Y., 2022. The first characterization of fog microphysics in the United Arab Emirates, an arid region on the arabian peninsula. Earth Space Sci. 9 (2) https://doi.org/10.1029/2021EA002032.

Williams, E., Nathou, N., Hicks, E., Pontikis, C., Russell, B., Miller, M., Bartholomew, M. J., 2009. The electrification of dust-lofting gust fronts ('haboobs') in the Sahel. Atmos. Res. 91 (2), 292–298. https://doi.org/10.1016/j.atmosres.2008.05.017.

Yair, Y., Yaniv, R., 2023. The effects of fog on the atmospheric electrical field close to the surface. Atmosphere 14 (3), 549. https://doi.org/10.3390/atmos14030549.

Yang, D., Ritchie, H., Desjardins, S., Pearson, G., Macafee, A., Gultepe, I., 2010. High-resolution GEM-LAM application in marine fog prediction: evaluation and diagnosis. Weather Forecast. 25, 727–748. https://doi.org/10.1175/2009WAF2222337.1.

Yaniv, R., Yair, Y., Price, C., Katz, S., 2016. Local and global impacts on the fair-weather electric field in Israel. Atmos. Res. 172–173, 119–125. https://doi.org/10.1016/j.atmosres.2015.12.025.

Zhang, M., Li, J., Li, C., He, F., Li, D., Yu, K., Pan, Y., 2023. Investigation of the effects of parallel electric field on fog dissipation. J. Phys. Appl. Phys. 56 (37), 375204 https://doi.org/10.1088/1361-6463/acd85c.